

## Supplementary data

### Efficient photocatalytic oxidative deamination of imine and amine to aldehyde over nitrogen-doped $\text{KTi}_3\text{NbO}_9$ under purple light

Zhuobin Yu,<sup>ab</sup> Xianmo Gu,<sup>\*ac</sup> Ruiyi Wang,<sup>ac</sup> Jie Wang,<sup>ac</sup> Jian Zhao<sup>d</sup>, LinJuan Pei<sup>ac</sup> and Zhanfeng Zheng<sup>\*ac</sup>

<sup>a</sup> State Key Laboratory of Coal Conversion, Institute of Coal Chemistry, Chinese Academy of Sciences, 27 South Taoyuan Road, Taiyuan 030001, PR China

<sup>b</sup> Taiyuan University of Technology, Taiyuan 030024, China

<sup>c</sup> Center of Materials Science and Optoelectronics Engineering, University of Chinese Academy of Sciences, Beijing, 100049, P. R. China

<sup>d</sup> Tianjin Key Laboratory of Organic Solar Cells and Photochemical Conversion, School of Chemistry and Chemical Engineering, Tianjin University of Technology, Tianjin, 300384, China

<b>Supplementary data</b> .....	1
Experimental section .....	2
Figure S1 The crystal structure of $\text{KTi}_3\text{NbO}_9$ .....	3
Figure S2 The optimized calcination time for nitrogen-doped KTNO in air were determined by the photocatalytic activity (imine formation and deamination) .....	4
Figure S3 The output spectrum of colored LED light source utilized in this work. ....	5
Figure S4 $\text{N}_2$ adsorption–desorption isotherms of (a) KTNO, and (b) N-KTNO. ....	5
Figure S5 XPS spectra of KTNO and N-KTNO. ....	6
Figure S6 The photoluminescence (PL) spectra of KTNO and N-KTNO. ....	7
Figure S7 (a) The photo-current responses, (b) EIS Nyquist plots of KTNO and N-KTNO samples. ....	7
Figure S8 The influence of catalyst dosage on the photocatalytic activity for imine deamination. ....	8
Figure S9 The mass spectra of $\text{PhCH}=\text{NH}$ intermediate .....	9
Figure S10 Cycling performance of the N-KTNO photocatalyst for imine deamination. ....	10
Figure S11 The UV-Vis-DR spectra of N-KTNO photocatalyst and N-KTNO before and after <i>N</i> -benzylidenebenzylamine adsorption. ....	10
Figure S12 The ESR spectra of KTNO and N-KTNO. ....	11
Table S1 Photocatalytic the tandem reaction of benzylamine oxidative coupling and imine deamination over various photocatalysts .....	12
Table S2 The catalytic tandem reaction of benzylamine oxidative coupling and imine deamination over various materials .....	12
Table S3 The photocatalytic tandem reaction of imine formation and deamination from various amines over N-KTNO. ....	13

## Experimental section

### Photoelectrochemical measurements

Test condition for photo-current response and Mott-Schottky plots 0.1M Na<sub>2</sub>SO<sub>4</sub> aqueous solution with the pH maintained at 6.8. Test condition for electrochemical impedance spectroscopy (EIS)] in 0.1 M KCl, 2 mM K<sub>3</sub>[Fe(CN)<sub>6</sub>] and 2 mM K<sub>4</sub>Fe(CN)<sub>6</sub>·3H<sub>2</sub>O electrolyte. ) The photo-current response were collected under purple light irradiation (light on/off cycle: 60s). The Mott-Schottky were carried out at a frequency of 1000 Hz. A platinum wire and an Ag/AgCl (saturated KCl) electrode were used as the counter electrode and reference electrode, respectively.

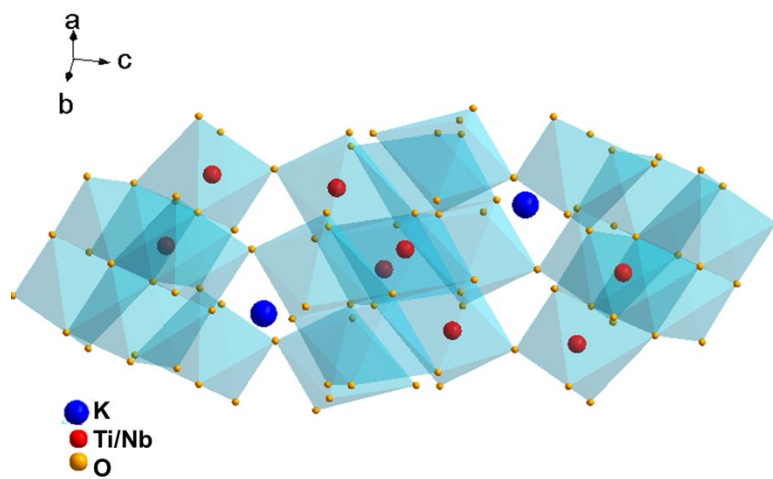


Figure S1 The crystal structure of  $\text{KTi}_3\text{NbO}_9$ .

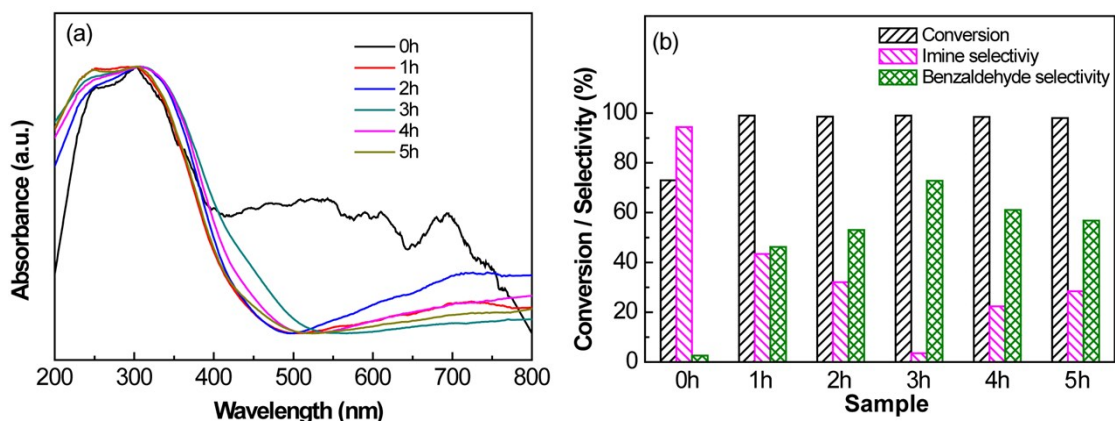


Figure S2 The optimized calcination time for nitrogen-doped KTNO in air were determined by the photocatalytic activity (imine formation and deamination).

The optimized calcination time for nitrogen-doped KTNO in air were determined by the photocatalytic activity: (a) UV-vis-DR spectra (b) Benzylamine conversion, imine selectivity, benzaldehyde selectivity over N-KTi<sub>3</sub>NbO<sub>9</sub> (labeled as N-KTNO) photocatalyst obtained with different calcination time in the air at 500 ° C

The UV-Vis-DR spectra of N-KTNO-0h sample is obviously different from other samples but it cannot catalyze the selective aerobic oxidation of benzylamine to benzaldehyde via PhCH=NH intermediate in one pot. The absorption edges of N-KTNO-3h in UV-Vis-DR spectra slightly red shift and corresponding photocatalytic deamination efficiency is much higher compared with other samples (N-KTNO-2h, N-KTNO-4h and N-KTNO-5h). This because the optimized annealing time in air after NH<sub>3</sub>-treatment is essential to preserve the original phase and obtain optimized nitrogen dopant to inhibit the recombination of photogenerated electrons and holes, which is in agreement with references. (1) Therefore, the calcination time of 3 h at 500°C in air is chosen.

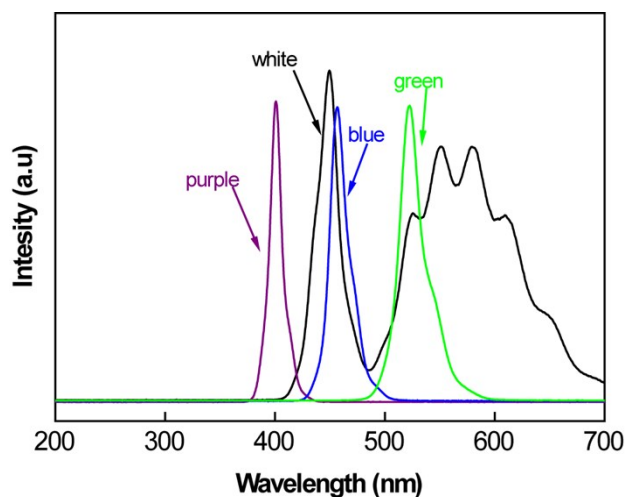


Figure S3 The output spectrum of colored LED light source utilized in this work.

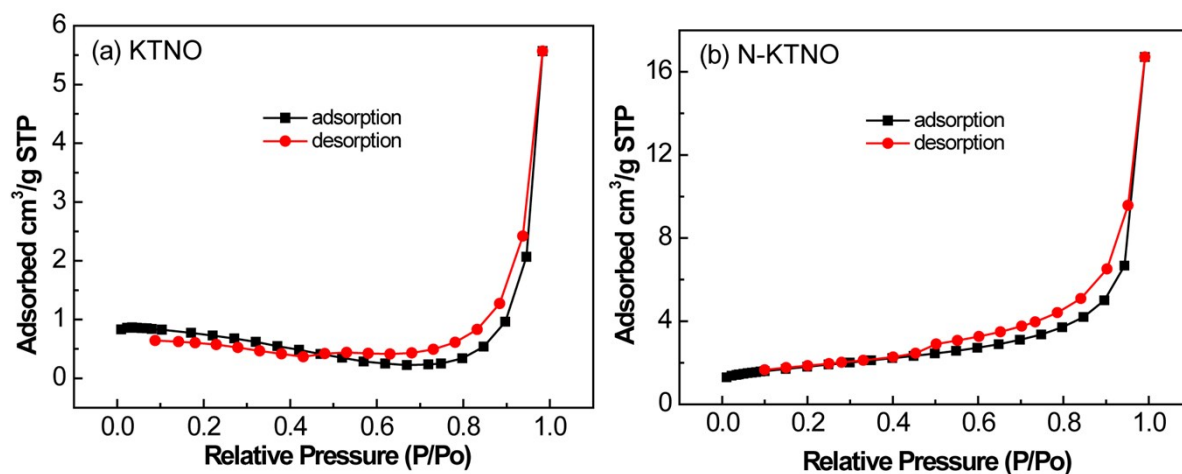


Figure S4  $N_2$  adsorption–desorption isotherms of (a) KTNO, and (b) N-KTNO.

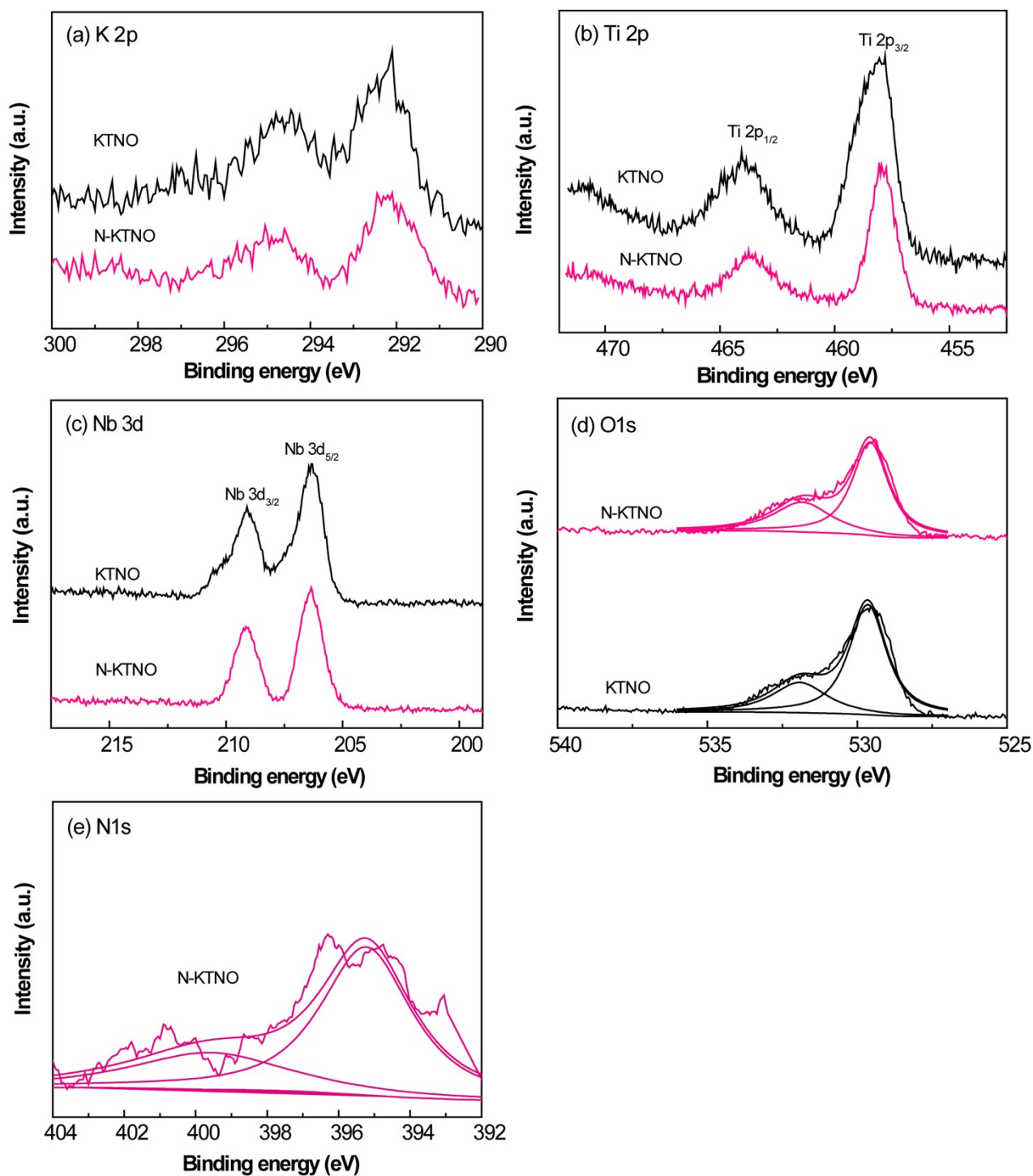


Figure S5 XPS spectra of KTNO and N-KTNO.

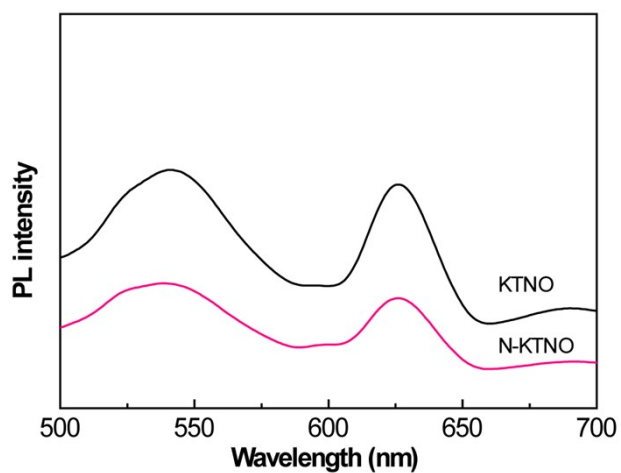


Figure S6 The photoluminescence (PL) spectra of KTNO and N-KTNO.

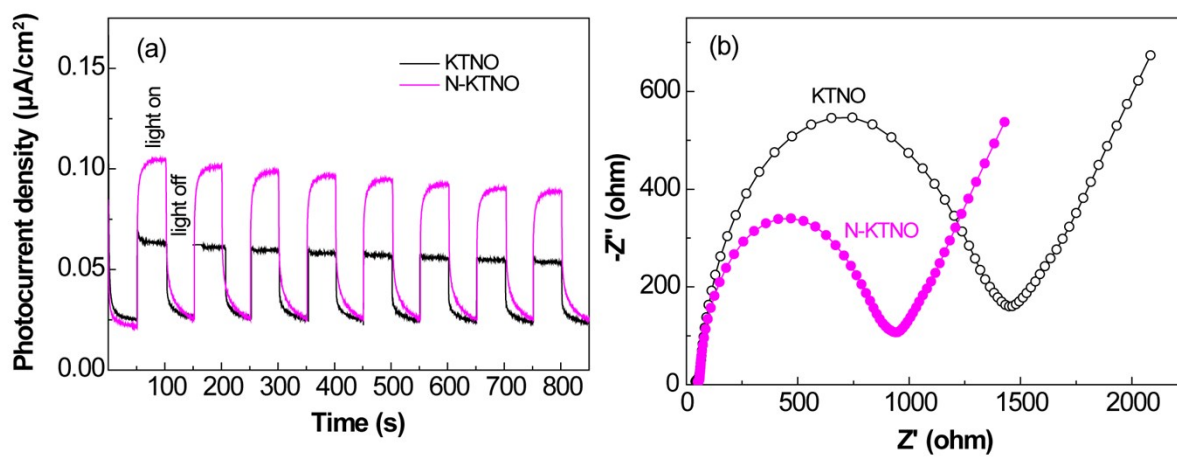


Figure S7 (a) The photo-current responses, (b) EIS Nyquist plots of KTNO and N-KTNO samples.

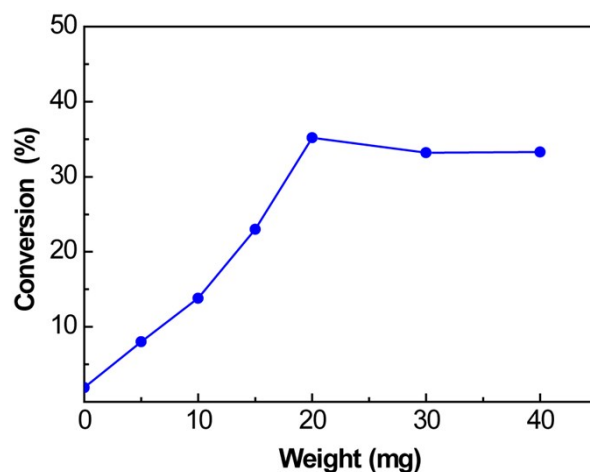


Figure S8 The influence of catalyst dosage on the photocatalytic activity for imine deamination.

Reactions: 3h, 80 °C, 200 mW/cm<sup>2</sup> purple light.

Figure S4 shows the slightly increase of specific surface area from 2.08 to 6.20 cm<sup>2</sup>/g for KTNO and N-KTNO. To investigate the influence of specific surface area on photocatalytic activity, the photocatalytic imine deamination as the function of catalyst dosage was obtained in Figure S8. As shown in Figure S8, the imine conversion rate increases linearly from 1.9 % to 35.2 % as increasing catalyst dosage from 0 to 20 mg. After 20 mg, no obvious difference was observed for the imine conversion over N-KTNO. This result indicates the there exists the optimal catalyst dosage while excessive catalyst should not provide contribution for imine deamination over N-KTNO photocatalyst.

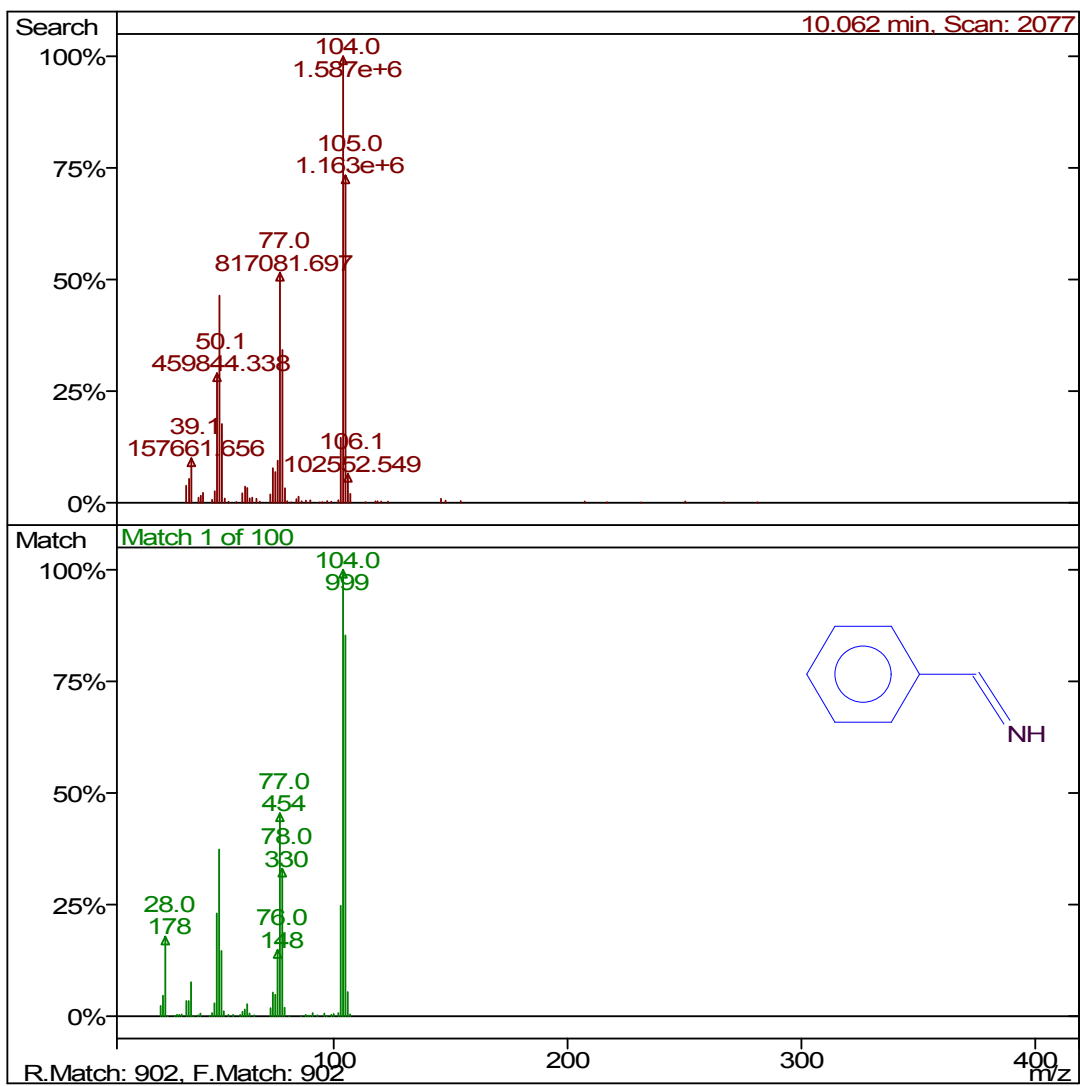


Figure S9 The mass spectra of PhCH=NH intermediate.

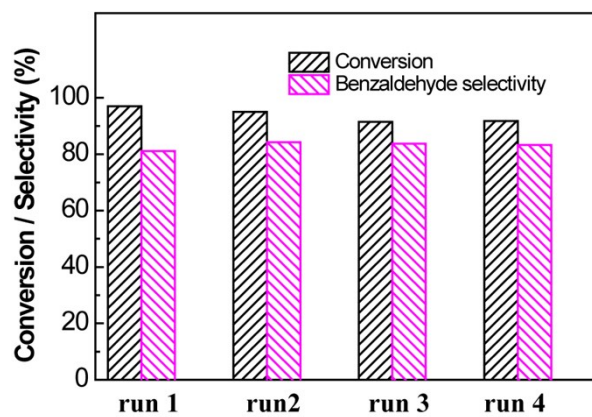


Figure S10 Cycling performance of the N-KTNO photocatalyst for imine deamination.

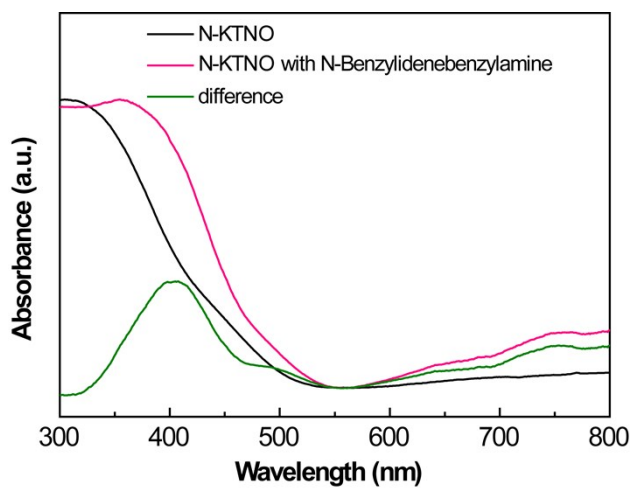


Figure S11 The UV-Vis-DR spectra of N-KTNO photocatalyst and N-KTNO before and after *N*-benzylidenebenzylamine adsorption.

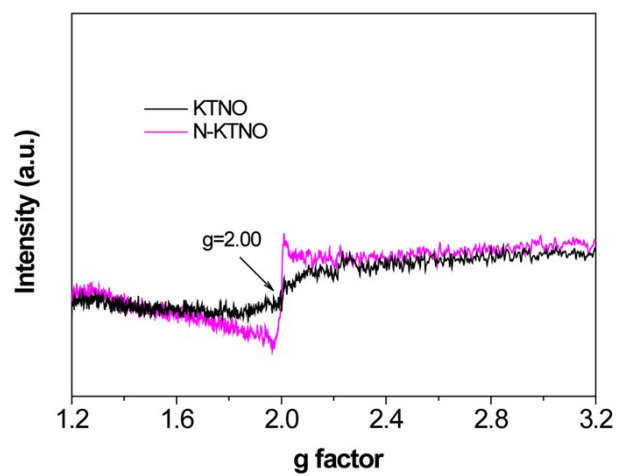


Figure S12 The ESR spectra of KTNO and N-KTNO.

In Fig. S12, the obvious signal centered at  $g=2.00$  is found for N-KTNO while a weak signal is found for KTNO, indicating the formation of more oxygen vacancies for N-KTNO than KTNO (2).

Table S1 Photocatalytic the tandem reaction of benzylamine oxidative coupling and imine deamination over various photocatalysts

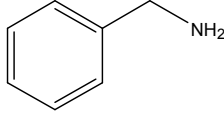
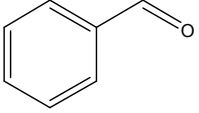
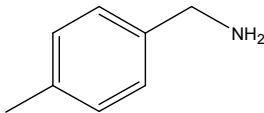
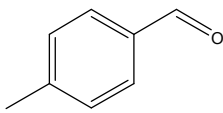
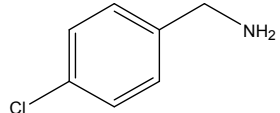
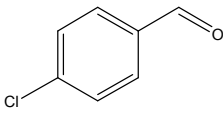
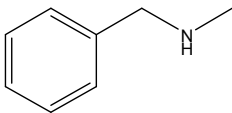
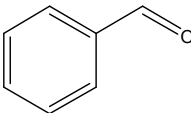
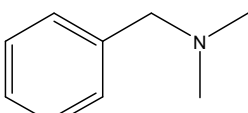
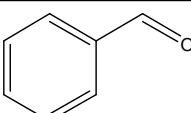
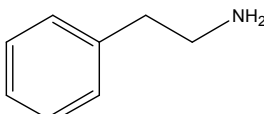
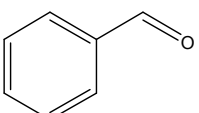
Entry	Photocatalyst	Conversion (%)	Selectivity/ Benzaldehyde (%)	Selectivity/ Imine (%)	Benzaldehyde yield (mmol mol <sub>catalyst</sub> <sup>-1</sup> )
1	-	8.55	0.93	97.9	
2	KTNO	55.22	1.54	96.05	14.92
3	N-KTNO	99	72.8	3.5	1210.81
4	TiO <sub>2</sub>	99	62.11	11.27	196.76
5	Nb <sub>2</sub> O <sub>5</sub>	99	40.89	52.0	430.72

The yield of benzaldehyde over N-KTNO is 1210 mmol/mol<sub>catalyst</sub>, much higher than those over TiO<sub>2</sub> (197 mmol/mol<sub>catalyst</sub>, Table S1 entry 4) and Nb<sub>2</sub>O<sub>5</sub> (430 mmol/mol<sub>catalyst</sub>, Table S1 entry 5). The difference in photocatalytic activity may be attributed to intrinsic crystal structure, leading to the change of band gap and number oxygen vacancies. (3)

Table S2 The catalytic tandem reaction of benzylamine oxidative coupling and imine deamination over various materials

Entry	Catalyst	Time(h)	Benzaldehyde Yield (%)/rate (%/h)	Imine Yield (%) /rate (%/h)	Temp(°C)/oxidant
1	N-KTNO	12	72.1/6.0	3.5/.03	80/O <sub>2</sub>
2 <sup>(4)</sup>	ortho-naphthoquinone	36	67.0/1.9	—	80/air
3 <sup>(3)</sup>	CeO <sub>2</sub> /CuO	36	<20/<0.6	80.0/2.2	110/air
4 <sup>(5)</sup>	N-bromosuccinimide	48	10.0/0.2	—	100/TBHP

Table S3 The photocatalytic tandem reaction of imine formation and deamination from various amines over N-KTNO.

Entry	Substrate	Conversion (%)	Selectivity/ imine (%)	Selectivity/ aldehyde (%)
1		99	3.5	 72.8
2		99	4.6	 71.7
3		98	28.9	 55.9
4		90	4.5	 67.4
5		90.5	3.12	 73.0
6		94.5	8.7	 20.1

## Reference

1. Park H, Song T, Paik U. Porous  $\text{TiNb}_2\text{O}_7$  nanofibers decorated with conductive  $\text{Ti}_{1-x}\text{Nb}_x\text{N}$  bumps as a high power anode material for Li-ion batteries. *Journal of Materials Chemistry A*. 2015;3(16):8590-6.
2. Wang S, He T, Chen P, Du A, Ostrikov K, Huang W, et al. In situ formation of oxygen vacancies achieving near-complete charge separation in planar  $\text{BiVO}_4$  photoanodes. *Advanced Materials*. 2020;32(26):2001385-94.
3. Al-Hmoud L, Jones C. Reaction pathways over copper and cerium oxide catalysts for direct synthesis of imines from amines under aerobic conditions. *Journal of Catalysis*. 2013;301:116-24.
4. Golime G, Bogonda G, Kim H, Oh K. Biomimetic oxidative deamination catalysis via ortho-naphthoquinone-catalyzed aerobic oxidation strategy. *ACS Catalysis*. 2018;8(6):4986-90.
5. Gong L, Xing L, Xu T, Zhu X, Zhou W, Kang N, et al. Metal-free oxidative olefination of primary amines with benzylic C-H bonds through direct deamination and C-H bond activation. *Organic & Biomolecular Chemistry*. 2014;12(34):6557-60.